Abyssinia Journal of Engineering and Computing Abyss. J. Engg & Comput., vol.4 , no.1, 2024, 42-55

Numerical and Experimental Performance Study of Bladeless Wind Turbine

Esskindir Demeke Geto[a*], Tesfaye Kebede Ali [b], Osman Mohammed Damtew [a], Eyob Hailemichael Yimer [a]

[a] Department of Mechanical Engineering, Wollo University, Kombolcha Institute of Technology, Ethiopia.
[b]Department of Mechatronics Engineering, Wollo University, Kombolcha Institute of Technology, Ethiopia.

DOI:
https://doi.org/10.20372/ajec.2024.v4.i1.1094

©2024 Kombolcha Institute of Technology, Wollo University

Open Access

ISSN : 2788-6239 (Print)
ISSN: 2788-6247 (online)

*Corresponding Author: esskindir@kiot.edu.et

ABSTRACT

Bladeless Wind Turbines (BWTs) represent an innovative and environmentally friendly approach to wind energy conversion, utilizing vortex-induced vibrations rather than traditional blades. This study aimed to evaluate the performance of BWTs by investigating key aerodynamic parameters through both numerical simulations and experimental methods. A comprehensive 3D analysis was conducted using the k-ω SST turbulence model in ANSYS FLUENT, alongside a 2D Fast Fourier Transform (FFT) analysis in Tecplot. These analyses provided valuable insights into critical factors such as frequency synchronization, amplitude ratios, and force coefficients. A prototype was 3D-printed and tested in a wind tunnel to validate the theoretical findings. The experimental results demonstrated a maximum amplitude ratio of 0.155 and a nominal power output of 0.43 milliwatts at a wind speed of 3 meters per second, suggesting significant potential for small-scale applications. Additionally, direct amplitude measurements were taken using a custom-designed stand to corroborate the 2D FFT results. The overall findings indicate that BWTs could serve as effective alternatives for urban environments, where traditional wind turbines may not be feasible The findings highlight BWTs as promising alternatives for urban settings, with further optimization needed for increased efficiency.

Keywords: Bladeless wind turbine, Vortex induced vibration, Wind energy, CFD, Amplitude, Frequency

1. INTRODUCTION

Unlocking the potential of wind energy has been done for decades now [1]. The kinetic energy from the wind is imparted to wind turbines which will then convert it to electrical energy. This is the basic working principle of how wind turbines work. There are different classifications of wind turbines the most famous one though is the conventional three-bladed horizontal axis wind turbine (HAWT) [2,3]. This turbine has been serving for years traditional rotational wind turbines are somewhat unpopular due to certain drawbacks that arise from their large size. Issues such as their visual impact and the noise they generate pose significant challenges to installing wind turbines in proximity to densely populated

areas or important natural sites. On the other hand, reducing the size of wind turbines can make them less economically viable compared to other energy sources or alternative land uses, often resulting in limited application for small-scale distributed power generation [4]. For these reasons, in recent years, there has been a growing interest in new concepts of wind power generators, particularly in the application of flow-induced vibrations or oscillations as an alternative mechanism for harnessing wind power [5-7]. In contrast to conventional wind turbines, these newly developed mechanisms do not involve any rotational motion. Their functionality is based on the phenomenon of vortex chains, which occur when a fluid or gas flows around elongated cylindrical structures oriented perpendicular to the direction of the continuous medium's movement. Vortices separate on both sides of the body in an alternating manner [8]. Following this separation, two chains of vortices form on the body's rear side, with the direction of rotation in one chain being opposite to that of the other. Figure 1, shows the trajectory of vortices commonly referred to as Karman's path [9].

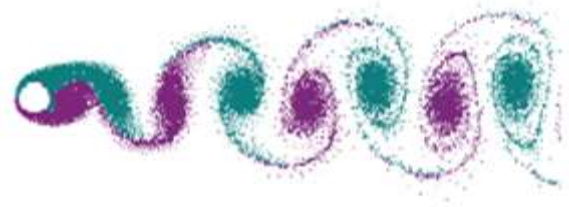

Fig 1. Karman's path indicating the vortex street effect [9]

The phenomenon, which happens when the shedding frequency of the wind coincides with the intrinsic frequency of BWT, is known as lock-in or synchronization [10,11]. In this stage of the flow, the turbine can extract the most energy. Low cut-in speed, high energy density, and a promising energy future are some advantages of this type of energy harvester [12]. Recently, numerous researches have been conducted regarding bladeless wind turbines [13,14].

Vishnu. M.R.Vishnu et al. [7] designed and fabricated a bladeless windmill. They have preferred a conical mast shape as their harvester. Their design incorporates theoretical analysis to fix the dimensions of their main components. They have reported that their prototype can generate 2 to 4V of current within the respective wind speed ranges of 3 to 5m/s. David Jesús and Yáñez Villarreal [8] introduced their novel unconventional energy harvester. They have performed a comprehensive numerical and experimental analysis. They performed computational analysis using the Altair CFD package for dimensional analysis which is assisted by theoretical analysis. Wind tunnel tests were also done on their model. They have used electromagnets to generate electricity. Their study affirmed the hypothesis of energy harvesting from aeroelasticity.

S.V.Goryachev [9] designed a tapered mast BWT and performed a theoretical analysis. As per their study the turbine has a potential but has a huge setback with 30% reduction in electric generation capacity in comparison to HAWT. However, they have mentioned that the robust nature of the turbine can compensate this drawback along with its low manufacturing, installation, and maintenance cost, as per their statement. Ganesh B.Vyawhare et al. [15] have conducted a CFD strength analysis of the mast and made a detailed explanation on the state of art of how the turbine works. Additionally, they have performed a theoretical parametric study. They concluded that the turbine has huge advantages over the conventional wind turbines. Abhijit Mane et al. [16] designed a bladeless wind turbine with a gyro E-generator. They have developed a 3D printed prototype and integrated it with a gyro E-generator. As per, their findings the removal of rotating mechanical and electrical parts in their design led to a superior economic advantage over the conventional wind turbines with an estimated 53% reduction in maintenance cost.

Gang Hu et al. [17] conducted experimental investigations on different BWT models they designed. They

have introduced different rod-shaped attachments such as rectangular, circular, and triangular on the basic cylindrical mast. The attachments were placed strategically at different azimuth locations. According to their findings, the turbine mast with triangular attachments placed at 600 on it performed well in comparison to the circular and rectangular attachments in terms of voltage output. Research related to bladeless wind turbines has been conducted and most of them are still trying to find the efficient mast type and generator type. In most of the studies, the objective revolves around the working principle of the bladeless wind turbine. They lack in-depth analysis of the parameters like amplitude ratio, lock-in frequency ranges, and other aerodynamic parameters of the bladeless wind turbine. However, this study aims to bridge this literature gap. So, the objective of this study is to (1) estimate the amplitude ratio and frequency range of the turbine numerically and experimentally at different wind speed values, (2) find the aerodynamic lift force coefficient, (3) calculate the nominal power output of the turbine, and (4) analyze the flow patterns of the flow over the mast from the contours. To achieve these the study employs Reynolds Averaged Navier-Stokes (RANS) equations and the SST k-ω turbulence model to analyze force coefficients in the proposed 3D model. In addition, the fast Fourier transform (FFT) approach is employed in an analogous two-dimensional cross-sectional model to estimate characteristics like vibration magnitudes and frequency ranges. In addition, computational fluid dynamics (CFD) findings were compared to experimental results. The main objective of the study consisted of amplitude measurements at various wind speeds, utilizing a unique amplitude-measuring platform through both computational and experimental methods.

2. MATERIAL AND METHODS

2.1 Materials used for the investigation

This section provides the methods used to perform the studies. Both numerical and experimental methods are presented. Two numerical methods are employed for in-depth analysis separately for the 3D model and the 2D model. The experimental method utilized is the wind tunnel test to find the force coefficient values. And, amplitude measurement along with estimating the frequency, using a custom-made amplitude measuring stand. To perform the experimental tests, it was mandatory to develop a model. To do that, a 3D printing technique was employed. The printing material used was PLA (Poly Lactic Acid). The domain and dimensions used for the studies are identical, meaning that the numerical fluid domains for computational study were made exact replicas of the physical (experimental) domains. So, the model used is exactly similar which is studied virtually and experimentally. Figure 2, below shows the perspective parametric view of the hollow mast.

2.1.2 Dimension of the VBWT mast

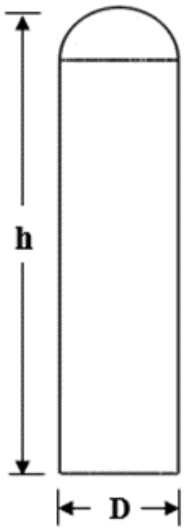

Fig2. Schematic diagram of the proposed BWT mast

A fixed parameters approach and iterative methods were employed to fix the dimensions of the mast. These methods are parts of a simple harmonic model, which has been used to study oscillators [4,18]. Dimensionless parameters like mass ratio, aspect ratio, and density of the mast are fixed using previous studies [19-22]. Then, the mast's height, thickness, and diameter are iterated

using those dimensionless parameters and flow. The dimensions of the mast including, its height (h), diameter (D), and thickness (t), are: h (mm) = 170, D (mm) = 40, and t (mm) = 4.

2.2 Numerical methods used for model development

In this section, the numerical studies used in the study for the 3D model, i.e., RANS, and the 2D model, i.e., FFT (Fast Fourier Transform), were discussed in detail. These numerical studies were conducted using ANSYS FLUENT 2023 R1.

2.2.1 Reynolds Average Navier-Stokes (RANS) methods applied to the 3D model

Flow over the mast is identical to flow over a cylinder. Implies the flow is highly unsteady and turbulent with time. So, to solve such a like flows there are different numerical schemes. RANS models are well-suited ideal solvers [23]. From, the two-equation RANS models the, k-ω SST was selected for this study. This is because of the accuracy of this turbulence model in solving near-wall shear stress forces [24]. Additionally, it is particularly suited for flow over curved surfaces with high adverse pressure gradients, like flow over a cylinder [25]. So, the k-ω SST two-equation model is used for estimating the flow parameters in this study.

Governing equations supporting model development:

The numerical model (k-ω SST) solves the motion of a viscous fluid using the incompressible Reynolds-Averaged Navier-Stokes (RANS) equations.

$$\frac{\partial u_i}{\partial t} + u_j \frac{\partial u_i}{\partial x_j} = -\frac{1}{\rho}\frac{\partial p_{rgh}}{\partial x_i} + \nu \frac{\partial^2 u_i}{\partial x_j^2} - \frac{\partial u_i' u_j'}{\partial x_j} \quad (1)$$

$$\frac{\partial u}{\partial x} + \frac{\partial v}{\partial y} = 0 \quad (2)$$

Where u_i are the Cartesian components of the fluid velocity, ρ is the fluid density, p_{rgh} is the pressure over the hydrostatic pressure, and ν is the kinematic viscosity. $u_i' u_j'$ is the Reynolds stress component. The components of the viscous stress tensor τij in are defined as:

$$\tau_{ij} = 2\mu S_{ij} + \lambda \frac{\partial v_k}{\partial x_k}\delta_{ij} = 2\mu S_{ij} - \left(\frac{2\mu}{3}\right)\frac{\partial v_k}{\partial x_k}\delta_{ij} \quad (3)$$

And, the components of the strain-rate tensor are given by:

$$S_{ij} = \frac{1}{2}\left(\frac{\partial v_i}{\partial x_j} + \frac{\partial v_j}{\partial x_i}\right) \quad (4)$$

2.2.1.1 Mesh creation and Boundary conditions applied to the analysis

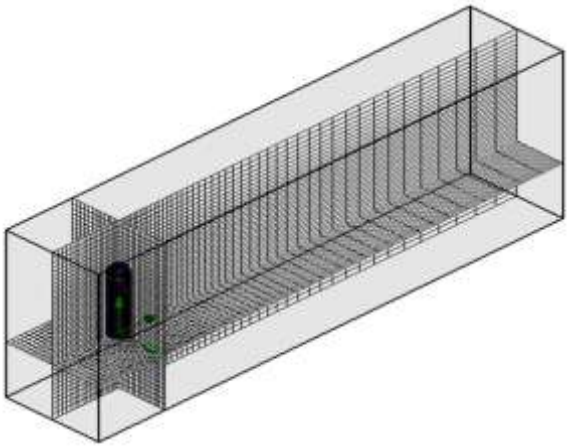

Fig 3. Mesh topology generated in the study

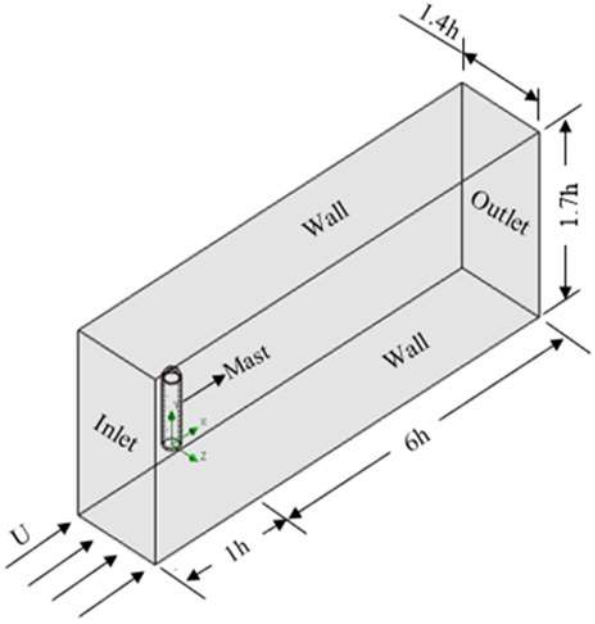

Fig 4. Boundary conditions applied in the study

For a hexahedral mesh with a 1 mm element size on the mast and a 5 mm element size for the domain, the mesh consisted of 3,256,849 elements. Figure 3 shows the mesh topology of the domain used in the study from various perspectives.

The boundary conditions used in the study are shown in Figure 4; transient velocity inlet, pressure outlet, cylindrical mast, and no-slip wall conditions. The numerical setup utilized for studying the effect of the flow on the 3D model is summarized in Table 1.

Table 1. Overview of the numerical setup employed in the study for the 3D model

=

Setup for 3D model	Parameters for 3D model
Software package	ANSYS FLUENT 2023
Flow type	Turbulent
Turbulence model	k-ω SST
Solver	Pressure based (Presto)
Initialization	Standard
Number of Iterations	20
Time step size (s)	0.0006
Number of time steps	2000

2.1.2 Configuration applied for the 2D model

The 2D study on the mast was nothing but an external flow over a circular cross-section. The method used in the study focused on estimating the amplitude ratio, maximum frequency range, and synchronization range. To do so, the FFT (Fast Fourier Transform) method was employed.

2.1.2.1 Mesh creation and boundary conditions applied for the 2D model analysis

Before running the calculation mesh generation, and selection of the physics were done. To permit mesh motion the dynamic mesh technique was employed on the fluid domain, which is shown in Figure 5. The mesh generated has an element size of 1 mm near the mast with 10 layers of inflation added and 5 mm for the rest of the domain. While generating the mesh the face meshing tool was used to increase the orthogonal quality of the mesh. The final mesh count for the 2D domain was 45,000 elements.

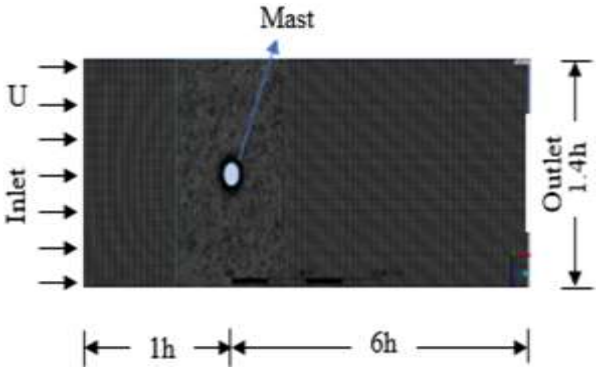

Fig 5. 2D mesh generation and boundary conditions applied in the study

The boundary conditions were also adjusted in alignment with the 3D study. The inlet of the flow to the domain was the velocity inlet. In consideration of the transient nature of the flow, the inlet velocity was set using a named expression, i.e.,

$$(10[m/s]\times(1-\exp(-Time/30[s])),$$

meaning that the velocity varied from 1 to 9 m/s with time. The outlet was a pressure outlet. Additionally, to fully analyze the flow, the motion of the mast was allowed. To do that, the dynamic mesh setting was adjusted using the six degrees of freedom setting, and the motion of the mast was controlled using a 'C' language-based UDF. The summary of the 2D model's numerical setup was presented in Table 2.

Table 2. Overview of the numerical configuration applied in the 2D model study

Setup (For 2D model)	Parameters for 2D model
Software package	ANSYS FLUENT 2023
Flow type	Turbulent
Physics	FFT
Mesh Type	Dynamic Mesh
Initialization	Standard
Number of Iterations	30
Time step size (s)	0.001
Number of time steps	1500

2.3 Experimental setup for measuring frequency and amplitude

In this section, the two experimental methods used to validate the numerical methods were discussed in detail. To perform the experiments, a 3D-printed model of the

turbine was used. The first experimental method was the classic wind tunnel experiment to find the force coefficients of the mast. The subsequent method was used to measure the remaining aerodynamic parameters, such as the amplitude and frequency of the mast at different wind speed values.

2.3.1 Wind tunnel experiment for determining lift and drag coefficients

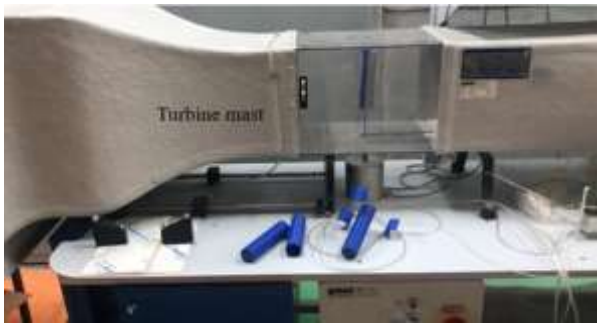

Fig 6. Wind tunnel testing experiment on the proposed BWT

For this study the wind tunnel test experiments were done using the HM 170 wind tunnel. This wind tunnel can achieve air velocity of 28 m/s [26]. The lift and drag force coefficients of the mast were measured at 5 m/s wind speed where frequency synchronization persists. Figure 6, below shows the experimental setup arrangement to perform the studies.

2.3.2 Experimental amplitude and frequency measurement

The remaining parameters, such as the maximum amplitude and frequency of the turbine at different wind speeds, were measured using a custom-made experimental setup.

This experimental setup consisted of a channel and a mechanical amplitude measuring stand. As shown in Figure 7, the measuring stand included the stand (220 mm×250 mm), scaled caches (100 mm × 20 mm) to measure amplitude at the top and the middle of the mast, pointers (1.5mm × 150 mm) to push the caches by translating the force of the mast under the applied wind force, an elastic compression spring (with 4 active coils and a 40 mm outer diameter) to connect the mast with the base, and the base (18 mm×100 mm× 220 mm) which supported the entire system. The channel was made from 3 mm thick sheet metal and was aligned with the numerical fluid domain, having specific dimensions of (240 mm×300mm×1200 mm).

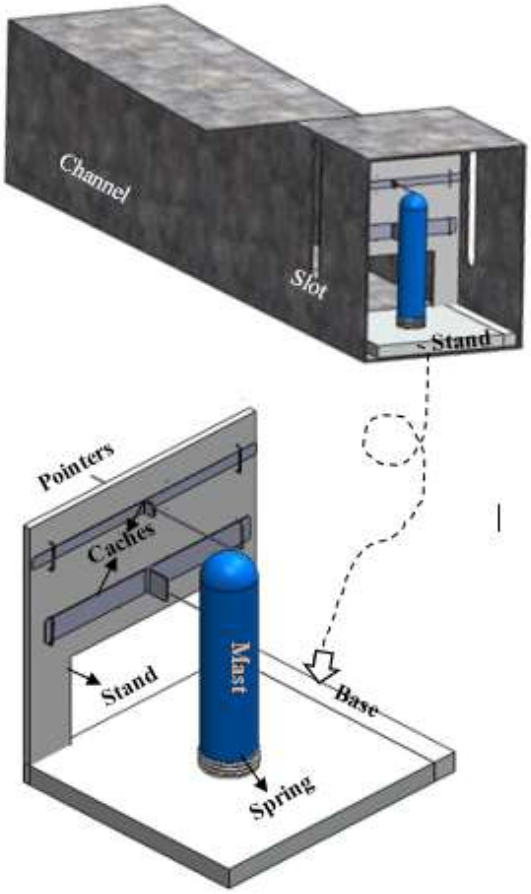

Fig 7. Experimental set for measuring oscillation amplitude and frequency

Additionally, to permit free movement of the caches during the oscillation of the mast, two parallel oppositely placed slots (8 mm × 200 mm) were made on the surface of the channel. The air was forced into the channel using a variable speed HP-1343 electric blower, which had a velocity range of 1 m/s to 9 m/s. To balance the concentration effect of the nozzle cross-section from the blower outlet, the blower was positioned 1.5 m away from the channel's inlet. The values of the wind speed

were measured just before the mast by an anemometer, which determined the position of the blower.

3. RESULTS AND DISCUSSION

This section provided the numerical and experimental results. The plots from the computational study (from the RANS analysis and the FFT analysis) were also presented, and the contours were discussed. Additionally, the plots of the experimental findings from the two experiments were used to validate the numerical results. Finally, the estimated power output from the results was also documented.

3.1 Outcomes of the numerical analysis

In this section, the results from the computational studies of the RANS K-ω SST model (in section 3.1.1) and FFT (in section 3.1.2) were presented. The results included respective velocities and other essential contours of the flow, which were helpful in analyzing the flow behavior.

3.1.1 Numerical results from the RANS analysis of the 3D model

The results from the RANS (k-ω SST) showed flickering hope regarding the proposed bladeless wind turbine. The contours in Figure 8, from the velocity streamline and pressure contours depict the formation of the vortex at the leeward direction of the mast.

Figure 8(a) shows the formation of two counter-rotating eddies, which were accountable for the formation of form drag. This was undesirable since they facilitated early boundary layer separation from the surface of the mast. If either the flow was not attached or did not reattach itself to the mast just after separation, the oscillation of the mast was intermittent. In other words, the oscillation in the drag direction was more dominant than that of the transverse direction oscillation. However, the magnitude of the transverse direction oscillation was twice that of the inline direction one. To utilize the energy from the vortices shedding from the surface of the mast continuously, the correlation length of the eddies should have been optimal.

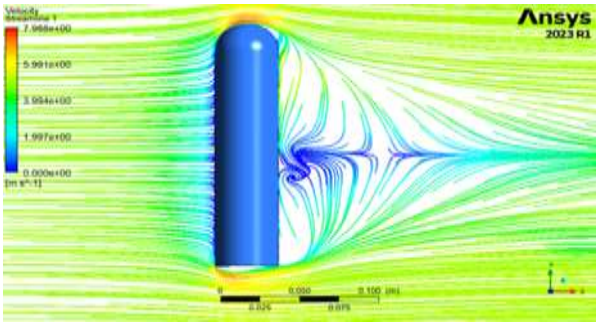

Fig 8a. Velocity streamline visualization

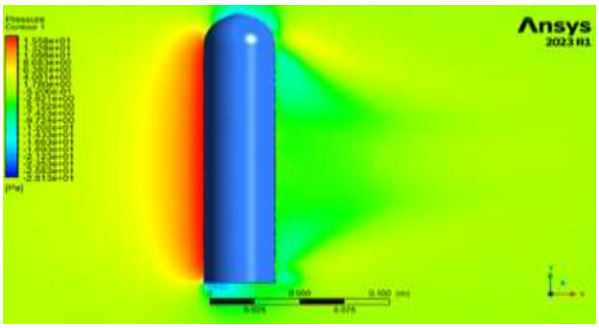

Fig 8b. Pressure contour visualization of the mast

In the case of this study, the correlation length of the eddies formed was elongated a little bit, which forced the incoming air particles to pass by without imparting their energy. Figure 8(b) was the pressure contour showing the formation of a static pressure line at the leading edge of the mast. As depicted in the contour, the inline direction oscillation was dominant.

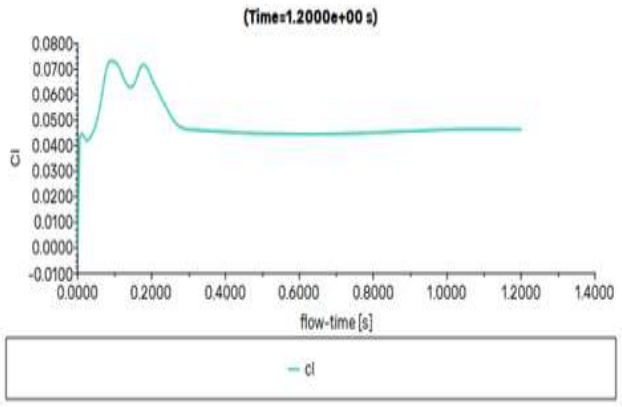

Fig 9. Lift coefficient of the mast
at a reference wind speed of 5 m/s

Figure 9 below presented the lift coefficient value at synchronization range wind speed, i.e., at 5 m/s wind speed, which was approximately 0.042, showcasing the blunt body effect. This value should have been higher to achieve continuous transverse force for oscillation.

Using this lift coefficient value, it was possible to estimate the theoretical amplitude ratio at the specified wind speed. Strouhal's relation played an important role in estimating the synchronization frequency. This relation depended on Strouhal's number, which varied with the flow regime that again depended on the Reynolds number. For the proposed turbine, the Reynolds number Re could be calculated using the Reynolds number relation [27]:

$$R_e = \frac{Inertial\ force}{Viscous\ force} = \frac{UD}{\nu} \quad (5)$$

For the 40 mm model subjected to a 5 m/s wind speed value, the Re value was found to be 13,605, where the flow was erratic and its regime was irregular. The value of the Strouhal number for a range of Reynolds numbers was shown about one another in Figure 10. As depicted in the plot, there were different flow regimes expressed in terms of Reynolds number, and they were related to their equivalent Strouhal number depending on the surface of the object subjected to the flow. In this study, the surface of the mast was smooth.

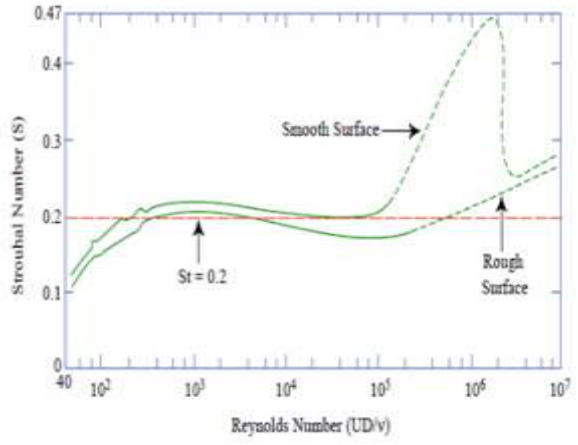

Fig 10. Strouhal number versus Reynolds number [28]

In this study, the Strouhal number was approximated at 0.2 for the calculated Reynolds number, as shown in the figure. The relationship between the Strouhal number and frequency enabled the determination of the lock-in frequency (fs) value. The Strouhal equation is written as:

$$St = \frac{f_s D}{U} \quad (6)$$

For the proposed mast's dimensions at the calculated synchronization range, the lock-in frequency was found to be 25 Hz. After finding the stiffness of the system, it was then possible to estimate the theoretical amplitude ratio value at the synchronization range using equation 7 [18]:

$$\left.\frac{A_y}{D}\right|_{f_s=f_y} = \frac{\rho U^2 C_L}{4k\xi} = \frac{C_L}{4\pi S^2 \delta_r} \quad (7)$$

Where ξ was the damping ratio, k was the stiffness of the system, and CL was the lift coefficient value of the mast. The value of the optimal damping ratio could be calculated using the following equation [4]:

$$\xi_{opt} = \frac{m^* \xi}{m^*} \quad (8)$$

$$m^* = \frac{m}{\rho_{air} D^2} \quad (9)$$

So, for the proposed mast, the mass ratio value was 21.5, which was desirable, since for a structure to vibrate in air, its range of mass ratio should be between 5 and 500 [19]. After inserting this value into equation 8, the optimal damping ratio value was 0.0093.

Finally, after estimating the stiffness of the system using equation 10 [4], it was possible to calculate the theoretical amplitude ratio of the mast using equation 10.

$$k = 4m\pi^2 {f_s}^2 \quad (10)$$

The modal stiffness of the proposed system was calculated as 1035.3 N/m. By substituting these values into equation 7, the theoretical amplitude ratio for the proposed mast was determined to be 0.033.

3.1.2 Numerical results from the FFT analysis (of the 2D model)

For a 15-second time frame, studies on the 2D model are conducted. The contours to analyze the behavior of the flow over the mast are presented at specific times. Figure 11 shows the stages of the flow in the velocity contour at different times, specifically (a) at 3 seconds, (b) at 7 seconds, (c) at 11 seconds, and (d) at 15 seconds. After 3 seconds of flow, the formation of vortices took place in the flow. Then, after a while, the shedding of vortices commenced downstream of the domain, as indicated by the vortices circled in Figure 11 (b).

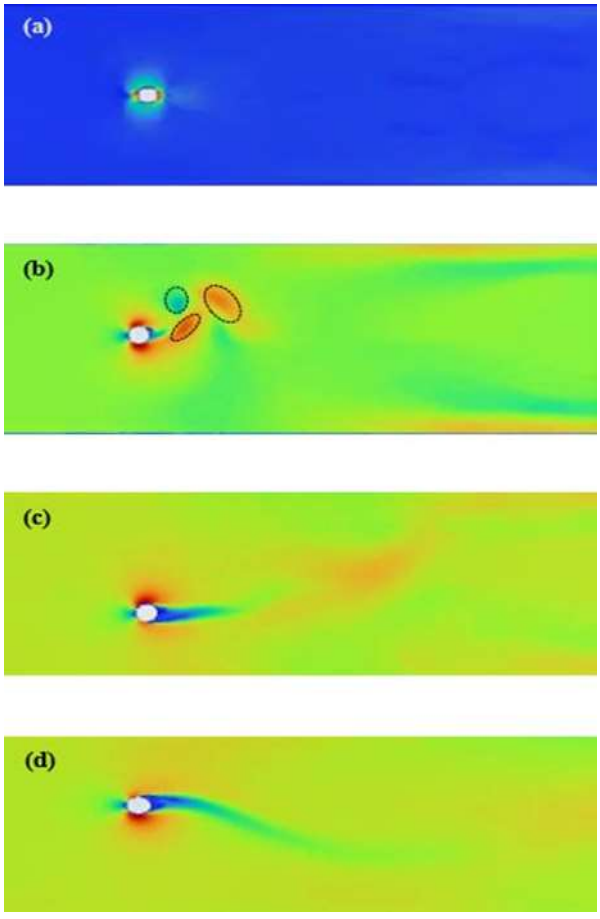

Fig 11. Velocity Contours of the Flow Over the Mast at Different Time Intervals. (a) Flow After 3 Seconds, (b) Flow After 7 Seconds, (c) Flow After 11 Seconds, (d) Flow After 15 Seconds

The shedding of vortices occurred due to the Coanda effect. This phenomenon happens as the fluid jet tends to stay attached to the curved surface of the mast, following the contour of the surface as it flows past.. This effect, along with the pressure drag, formed recirculating vortices. However, the incoming upstream fluid then forced these recirculating vortices away. The red color on the surface of the mast showed the stagnation pressure formed after the collision of air particles. This stagnation pressure was accountable for the oscillation of the mast. As the flow proceeded, the vortices were pushed farther away, as depicted in Figure 11 (c) and (d). In these figures, continual oscillation was also shown, with the pressure gradient alternating between the top and bottom surfaces of the mast. As the flow advanced, an elongated blue tail-like profile was formed, as shown in Figure 11 (c) and (d), indicating that the frequency of vortex shedding was minimized while the correlation length of the counter-rotating eddies at the back of the mast increased.

This facilitated the formation of adverse pressure and reduced the pressure gradient between the top and bottom surfaces of the mast, thereby reducing the oscillation amplitude and frequency of the mast. If the flow advanced further, the tuning of the shedding frequency of the air and the natural frequency of the mast would stop.

This behavior of the flow was also evidenced in the amplitude ratio vs. frequency plot of the mast generated in CFD post using Tecplot. This was because it was a complicated approach to measure the amplitude directly in ANSYS FLUENT. Therefore, it was mandatory to use another CFD post-processing tool to generate the Amplitude vs. Frequency plots and locate the maximum amplitude. Tecplot 360 EX 2023 R1 was used as the CFD post-processing tool. The results from ANSYS Fluent were exported in ".plt" format to Tecplot 360 EX, where the plots were generated.

Then, the magnitude of the oscillation with respect to frequency was plotted using this aforementioned tool. To do so, the pressure over the surface of the mast and

the y-velocity of the mast had to be found beforehand, which was done accordingly in ANSYS. The plot presented in Figure 12 was created by generating dependent variables like amplitude ratio, frequency, and phase from independent variables like pressure and vertex average y-velocity of the mast, and then using a probing tool followed by Fast Fourier Transform (FFT).

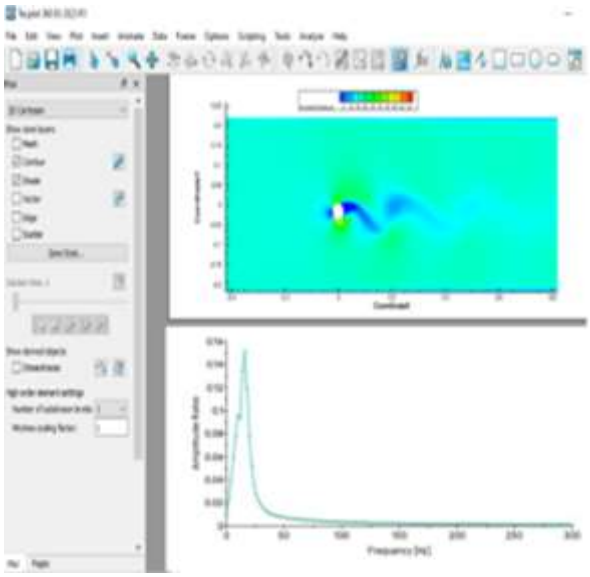

Fig12. CFD post-processing plot generated using Tecplot.

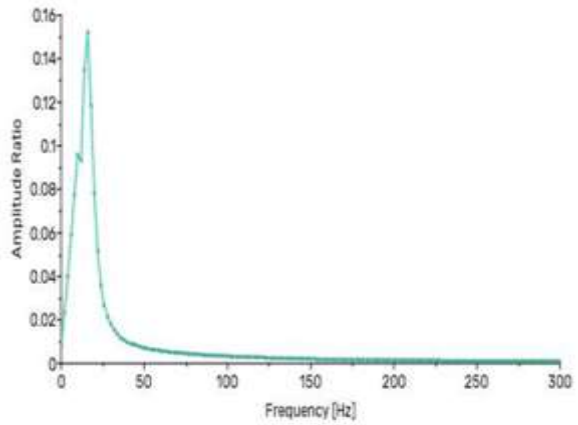

Fig 13. The plot of amplitude ratio versus frequency for the proposed BWT-

The amplitude ratio vs. frequency plot of the mast was depicted in Figure 13. The plot manifested that the synchronization range, where oscillation reached its maximum, was narrow and steep. Later, the flow and the mast lost their synchronization, and the oscillation dropped drastically. The approximate maximum amplitude ratio value for the mast was around 0.155. The oscillation became maximum in the range of 5 to 15 Hz and started to diminish after 50 Hz, becoming completely zero at a frequency of 200 Hz.

For a 5 m/s wind speed, the equivalent frequency was 25 Hz, as calculated in section 4.1. For this particular frequency, the respective amplitude ratio value ranged up to approximately 0.031. In comparison with the theoretical value of 0.033, the result from the FFT analysis was acceptable, with a marginal error of 6%.

3.2 Findings from the experimental studies

This section included the results from the 3D k-ω SST (lift coefficient) study, which were validated using the wind tunnel test results. The results from the numerical FFT analysis were compared with the direct amplitude measurement results, and the errors were presented.

3.2.1 Findings from wind tunnel testing

The wind tunnel tests were conducted at different wind speeds, and the lift coefficient values of the mast at these wind speeds were recorded. The results were then plotted in Figure 14. As displayed, the lift was augmented near a wind speed of 3 m/s, and it reduced when the wind speed increased further. This was due to early boundary layer separation, which resulted in a reduction in the lift coefficient.

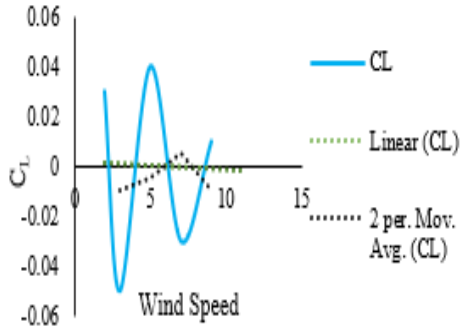

Fig 14. Lift coefficient (CL) versus wind speed for the proposed BWT mast

The results were almost identical to the numerical results of the RANS study. For instance, at a wind speed of 5 m/s, the lift coefficient value of the mast was found to be 0.042, while in the wind tunnel test, the respective value was 0.04. From this value, it was possible to calculate the theoretical amplitude ratio value using equation (7), since the mass of the mast and its modal stiffness value were identical to the numerical ones. The theoretical amplitude ratio value, depending on the experimental lift coefficient at 5 m/s, was 0.032. Thus, it was in between the results of the two numerical studies, and the error of the two numerical results was 3.1% relative to this experimental value.

3.2.2 Results of experimental measurements for amplitude and frequency

In this experiment, the amplitudes were directly measured for each respective wind speed. This was because the experimental setup was custom-made and able to measure the oscillation of the turbine at its top and middle directly using its scaled caches, as explained in section 2.3.2 and shown in Figure 7. The chart in Figure 15 showed the plot of amplitude values at the top and middle of the mast, while the bottom part of the mast was considered as it did not oscillate.

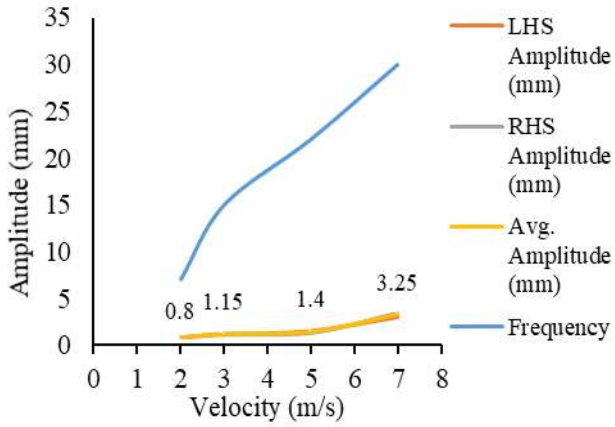

Fig 15. Plot of experimental oscillation amplitudes and frequencies of the turbine mast at varying wind speeds

As the results of the average oscillations from the Left-Hand Side (LHS) and Right-Hand Side (RHS) were called out in the chart, the average oscillation amplitude value at the top of the mast for a wind speed of 5 m/s was 1.4 mm.

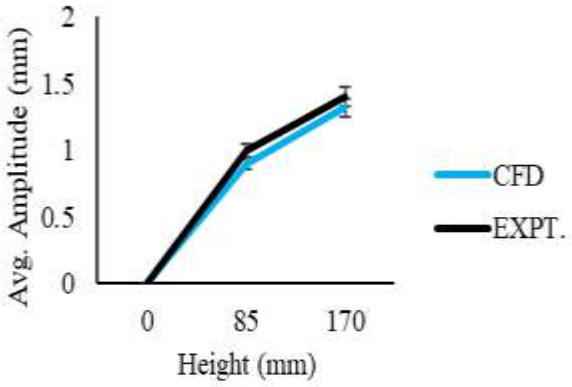

Fig 16. CFD and experimental plot of amplitude versus mast height at 5 m/s wind speed

This gave an amplitude ratio value of 0.035, which was a bit higher in comparison to the previous results. The amplitude as a function of the mast's height was plotted in Figure 16 below, showing that the oscillation increased exponentially from the base to the top of the mast.3.3 Energy conversion by the BWT.

For bladeless wind turbines, unlike the conventional ones, the energy extraction mechanism was different. Therefore, the nominal power and efficiency of the turbine calculation differed. According to some literature, the power and efficiency of BWT could be estimated using equations 11 and 12 [31].

$$P_{VBWT-fluid} = \frac{1}{2}\rho_{air}\pi C_l U^2 f_s y_{max} D h_m Sin(\phi) \quad (11)$$

$$\eta = \frac{f_s}{U} C_l \pi y_{max} Sin(\phi) \quad (12)$$

Where y_{max} was the maximum amplitude value, and ϕ was the phase angle of the flow relative to the mast. The maximum amplitude value was recorded at a wind speed of 3 m/s, where the amplitude ratio reached 0.155. This implied that for a 40 mm mast, its maximum equivalent amplitude value was 6.2 mm. The frequency at this particular wind speed was 15 Hz. Substituting these values resulted in the nominal maximum power generated

by the proposed BWT and its efficiency. The phase angle between the flow and the mast was considered to be 80° [4]. After substitution, the nominal power generated at maximum oscillation was 0.43 mW, and its efficiency was 0.38%.

4. CONCLUSION

This study conducted a comprehensive performance analysis of a bladeless wind turbine (BWT) using both computational and experimental methods. Numerical simulations through CFD tools, including ANSYS and Tecplot, were complemented by wind tunnel tests and a custom amplitude measurement setup to examine aerodynamic parameters, such as lift coefficient, amplitude ratio, frequency range, and nominal power output. Key findings from the study include:

Nominal power output and efficiency: The maximum power output reached 0.43 mW at a wind speed of 3 m/s, with an efficiency of 0.38%, indicating limited power generation compared to conventional HAWTs.

Amplitude Ratio and Frequency Range: The maximum amplitude ratio was 0.155, observed within the synchronization frequency range of 10–25 Hz, suggesting potential for small-scale energy harvesting through vortex-induced oscillations.

Lift coefficient: The average lift coefficient recorded was around 0.04, illustrating the drag body characteristics of the mast.

Velocity and pressure contours: The flow analysis revealed that vortex shedding and early boundary layer separation contribute to reduced energy extraction efficiency due to adverse pressure gradients.

While the current design shows promise, especially for low-noise and low-maintenance applications, the BWT requires further optimization. Future work could focus on structural modifications to the mast or using advanced materials to enhance efficiency and durability. Additionally, exploring a broader range of wind speeds and employing alternative CFD models may yield valuable insights for improved performance.

In summary, this study advances the understanding of BWT performance and identifies clear directions for making bladeless wind energy harvesters a viable alternative for sustainable energy generation.

REFERENCES

[1] T.Güney, “Renewable energy, non-renewable energy and sustainable development”, International Journal of Sustainable Development and World Ecology, vol.26, no.5, pp.’-389–397, 2019. doi: 10.1080/13504509.2019.1595214

[2] G. D. Rai, “Non-conventional sources of energy”, A Textbook for Engineering Students, Khanna Publishers, 6th edition, 2017.

[3] J.F.Manwell and J.G. McGowan, “Wind energy explained theory, design and application”, Wiley, second edition, 2017.

[4] Marco Boretto’, “Bladeless wind energy conversion”, Thesis, Politecnico Di Torino, Collegio di Ingegneria Meccanica, 2019. https://webthesis.biblio.polito.it/s cure/10738/1/tesi.pdf

[5] R.Haridass, K.S.Jayaram singh, T.Ramesh Kumar and B.Sabarish Kumar, “Design and fabrication of bladeless windmill”, 2018. doi: 10.12732/ijpam. v118i11.71.

[6] Soumya Ranjan Panda, “Design of a bladeless wind turbine”, International Journal of Scientific Development and Research, vol.2, no.4, pp.2455–2631, 2017.

[7] M.R.Vishnu, A.Akash, and J.J. Madhu, “Design and fabrication of bladeless windmill”, Karnataka State Council For Science and Technology, vol.9, no.6, pp.22862–22865, 2019.

[8] David Jesús and Yáñez Villarreal, “VIV resonant wind generators”, Vortex Bladeless S.L., vol.1, no.3, 2018.

[9] S.V.Goryachev and P.A.Kharchenko, “Use of bladeless generator in wind power”, International Conference on Industrial Engineering, Applications and Manufacturing, Proceedings, 2019.

[10] R.D.Gabbai and H.Benaroya, "An overview of modeling and experiments of vortex-induced vibration of circular cylinders", J Sound Vib, vol. 282, no.3 and no.5, pp.575–616, 2005. doi: 10.1016/j.jsv.2004.04.017

[11] R.N.Govardhan and C.H.K.Williamson, "Defining the modified Griffin plot in vortex-induced vibration: Revealing the effect of Reynolds number using controlled damping", vol.561, 2006. doi: 10.1017/S0022112006000310

[12] J.Wang, L.Geng, L.Ding, H.Zhu, and D. Yurchenko, "The state of the art review on energy harvesting from flow-induced vibrations", Elsevier, June 2020. doi: 10.1016/j.apenergy.2020.114902

[13] K.S.Kumar, "Design and fabrication of vortex bladeless windmill ", Int J Res Appl Sci Eng Technolgy, vol.6, no.3, pp.2407–2410, 2018. doi: 10.22214/ijraset.2018.3386

[14] K.Harshith, B.Santhosh Fernades, Tilak Raj, and P.R.Sreerama, "Bladeless wind power generation: An independent source for rural electrification", Project, Department of Electrical and Electronics Engineering, Srinivasa Institute of Technology. Reference No: 39S_BE_0635, 2016.

[15] G.B.Vyawhare, A.S.Kharde, R.R.Mohite and S. Singh, "Power generation by using vortex bladeless windmill", International Journal of Advance Research and Innovative Ideas in Education, vol.4=, no.5, 2020.

[16] A.Mane, M.Kharade, P.Sonkambale, S.Tapase, and S.S.Kudte, "Design & analysis of vortex bladeless turbine with gyro E-generator", International Journal Innovative Research in Science & Engineering, vol.3, no.4, 2017.

[17] G. Hu, K.T.Tse, M.Wei, R.Naseer, A.Abdelkefi, and K.C.S. Kwok, "Experimental investigation on the efficiency of circular cylinder-based wind energy harvester with different rod-shaped attachments", Appl Energy, vol.226, pp.682–689, Sep 2018. doi: 10.1016/j.apenergy.2018.06.056.

[18] R.D.Blevins, "Flow-induced vibration", Van Nostrand Reinhold and republished by Krieger Pub. Company, ISBN:1-57524-183-8, 2nd edition, Florida, 2001.

[19] K.N.Karagiozis, M.P.PaïDoussis, E.Grinevich, A. K. Misra and M.Amabili, "Stability and non-linear dynamics of clamped circular cylindrical shells in contact with flowing fluid", IUTAM Symposium on Integrated Modeling of Fully Coupled Fluid Structure Interactions Using Analysis, Computations, and Experiments, Conference proceedings, pp.375-390, 2003.

[20] Y.N.Chen, "Fluctuating lift forces of the karman vortex streets on single circular cylinders and in tube bundles: (Part 1)The vortex street geometry of the single circular cylinder", J. Eng. Ind., vol.94, no.2, pp.603-610, May 1972. https://doi.org/10.1115/1.3428206

[21] T.Sarpkaya, "Fluid forces on oscillating cylinders," Journal of the Waterway, Vol.104. no.3, pp.275–290, Aug 1978. https://doi.org/10.1061/JWPCDX.0000101

[22] M.L.Facchinetti, E.De Langre and F.Biolley, "Coupling of structure and wake oscillators in vortex-induced vibrations", Journal of Fluids and Structures, vol.19, no.2, pp.123–140, 2004. doi: 10.1016/j.jfluidstructs.2003.12.004.

[23] Roland Schiestel, "Modeling and simulation of turbulent flows", Wiley online library, ISBN:9781848210011, 1st edition, 2008.

[24] J.Blazek, "Computational fluid dynamics: Principles and applications", Companion Materials, Elsevier, 3rd edition, 2007. https://booksite.elsvier.com/9780080999951/

[25] F.R.Menter, “Two-equation eddy-viscosity turbulence models for engineering applications”, American Institute of Aeronautics and Astronautics, vol. 2, no.8, pp.1598–1605, 1994.
doi: 10.2514/3.12149

[26] Gunt Humberg, “Hm 170 open wind tunnel”, Equipment for Engineering Education, Manual,. Gerätebau GmbH, 2021.
https://www.gunt.de/en/products/open-wind-tunnel/

[27] M.M.Zdravkovich, “Conceptual overview of laminar and turbulent flows past smooth and rough circular cylinders”, Journal of Wind Engineering and Industrial Aerodynamics, vol.33, pp.53–62, 1990.

[28] M.Ahmed Elsayed and B. Mohamed Farghaly, “Theoretical and numerical analysis of vortex bladeless wind turbines”, Wind Engineering, Sage Publishers, 2022.
doi: 10.1177/0309524X221080468

[29] A.Barrero Gil, S.Pindado and S.Avila, “Extracting energy from vortex-induced vibrations : A parametric study”, Appl Math Model, vol.36, no.7, pp. 3153–3160,2012.
doi: 10.1016/j.apm.2011.09.085

[30] M.P.Paıdoussis, S.J.Price and E.De Langre, “Fluid structure interactions”, Cambridge University Press, 1st edition, vol.13, no.1, 2011.

[31] K.Raghavan and M.M.Bernitsas, “Experimental investigation of Reynolds number effect on vortex induced vibration of rigid circular cylinder on elastic supports”, Ocean Engineering, vol.38, no.5 and no.6, pp.719–731, 2011.
doi: 10.1016/j.oceaneng.2010.09.003